

# A Portable and Automated Postural Perturbation System for Balance Assessment, Training, and Neuromuscular System Identification

Albert H. Vette<sup>1,2</sup>, Egor Sanin<sup>2,3</sup>, Abdulkadir Bulsen<sup>2</sup>, Alan Morris<sup>2</sup>, Kei Masani<sup>1,2</sup>, and  
Milos R. Popovic<sup>1,2</sup>

<sup>1</sup> Institute of Biomaterials and Biomedical Engineering, University of Toronto  
164 College Street, Toronto, Ontario, M5S 3G9, Canada.

<sup>2</sup> Toronto Rehabilitation Institute, Lyndhurst Centre  
520 Sutherland Drive, Toronto, Ontario, M4G 3V9, Canada.

<sup>3</sup> Department of Mechanical and Industrial Engineering, University of Toronto,  
5 King's College Road, Toronto, Ontario, M5S 3G8, Canada.

Email: a.vette@utoronto.ca, egor.sanin@utoronto.ca, bulsen.abdul@torontorehab.on.ca,  
alan.morris@utoronto.ca, k.masani@utoronto.ca, milos.popovic@utoronto.ca

[www.toronto-fes.ca](http://www.toronto-fes.ca)

October 14, 2008

## Corresponding Author:

Albert H. Vette

Rehabilitation Engineering Laboratory

Institute of Biomaterials and Biomedical Engineering, University of Toronto

164 College Street, Toronto, Ontario, M5S 3G9, Canada

Phone: +1-416-964-7145

Email: a.vette@utoronto.ca

[www.toronto-fes.ca](http://www.toronto-fes.ca)

## ***Abstract***

**Background:** To date, a postural perturbation system capable of generating position-, velocity-, and force-controlled perturbations while being portable and suitable for use during various postural scenarios does not exist. Therefore, the purpose of the present study was to design, develop, and test a portable and automated postural perturbation system (PAPPS) that can be used to measure and train postural reactions during sitting, standing, and treadmill walking.

**Method of Approach:** The core component of the PAPPS was a linear actuator that provides horizontal perturbations. The actuator could generate arbitrary displacement, velocity, or force perturbations as a function of time. In addition, the PAPPS was able to measure the actuator's displacement, velocity, and load, which could be used to study postural perturbation responses. The height at which the PAPPS was delivering the perturbations could be easily adjusted to allow for different subject/patient anthropometrics and a wide range of postural scenarios such as sitting, standing, and treadmill walking. The PAPPS generated a peak displacement of 0.6 m, a peak velocity of 0.5 m/s, and a peak force of 600 N, which is more than sufficient to elicit high intensity postural perturbations. Multiple and nested safety circuits have been implemented into the PAPPS to ensure the safety of the subjects/patients during experiments and/or training.

To evaluate the accuracy and repeatability of the PAPPS during position-, velocity- and force-controlled perturbations, experiments were conducted using sinusoidal, impulse and ramp profiles as a function of time. Highly sensitive displacement and force sensors that were external to the PAPPS were used to determine the accuracy and repeatability of the proposed device. In addition, a case study was performed to demonstrate the

performance of the PAPPS during pseudorandom sinusoidal perturbations that were applied to a healthy individual during sitting.

**Results and Conclusions:** The accuracy and repeatability tests suggest that the PAPPS can generate reliable and high-precision displacement, velocity, and force perturbations. Potential applications of this system include, but are not limited to: (1) studies of postural response to various perturbation types and profiles in diverse subject populations during sitting, standing, and treadmill walking, and (2) training of postural balance in diverse patient populations during sitting, standing, and treadmill walking.

**Keywords:** Assessment, balance, device, perturbation, posture, training.

## I. INTRODUCTION

For a particular sensory environment, balance defines the ability to regulate the body's center of mass over the base of support during sitting, standing, or walking [1]. This intrinsic ability results from a combination of anticipatory and reactive balance control strategies. On the one hand, *anticipatory* control strategies are applied when the individual is able to predict the direction, intensity, and/or type of the imminent perturbation in order to minimize its impact on the body. *Reactive* control strategies on the other hand are utilized when the perturbation occurred unexpectedly and could not be anticipated. The goal of these strategies is to re-stabilize the body after the perturbation has challenged or compromised the individual's balance. Perturbations that elicit reactive – or feedback – control strategies are called *postural perturbations*. In order to study human responses to postural perturbations and to identify the role of the neuromuscular system in reestablishing postural stability, mostly *mechanical* perturbations have been used [2].

One of the most common experimental approaches for inducing postural perturbations is to mechanically perturb the support surface on which the subject is standing [3-7] or sitting [8-11], with the goal of characterizing the conditioned or unconditioned postural control system in various healthy or disabled populations. In this context, various studies have indicated the usefulness of multi-directional surface perturbations in studying postural responses and balance control strategies [12-17]. For example, using multiple perturbation directions in the pitch and roll planes, posture-correcting reactions in trunk and leg muscles were shown to have different sensitivities to the direction of external perturbation [12,13]. In addition, Henry *et al.* suggested that postural responses after translational surface perturbations depend on the various biomechanical constraints in the different planes of movement [14] and that their control is

characterized by a complex interaction of central and peripheral information [15]. Most recently, multi-directional surface perturbations were used to show that muscle synergies represent a general neural control strategy [16], but that such a global control pattern cannot be applied to all postural tasks [17]. Besides the surface perturbations, postural perturbations have also been applied directly to the trunk in order to quantify human trunk stiffness [18,19] and postural reflex properties [20-22] or to determine the effect of external loads on lumbar spine stability [23-26], muscle activation patterns [27-30], and body kinematics [27,30]. Similarly, subjects have been perturbed to characterize protective stepping responses in young and older adults [31,32] or to study falls in the anterior direction after perturbation of a forward leaning posture [33,34].

In the described studies, the applied perturbations were executed by either displacing the body of the subject directly (kinematics control) or by exerting or releasing a load that was attached to the subject (force control). In most cases, the perturbations exhibited a step profile [4-6,8-17,23-27,29,31-34], although impulse [19,21,30], sinusoidal [18,28], and randomized [3,4,7,20,22] profiles have been used as well. After carefully scrutinizing the perturbation devices that were applied in the aforementioned studies, one can conclude that only the perturbation *platforms* appear to be capable of delivering different perturbation profiles [3,4,7]. In fact, several types of support surface perturbation platforms have been developed with the capability of delivering perturbations via toe-up/down rotation, anterior/posterior translation, continuous sinusoidal translation, and multi-directional surface translation. Note that one of the most recent developments for standing applications, the *Research Platform* by Neurocom (Oregon, USA) and AMTI (Massachusetts, USA), can additionally measure the ground reaction forces and the body's center of pressure via two independent force plates [35]. The main limitation of such

perturbation platforms is, however, that they are expensive and typically fixed to one location (i.e., not portable). The devices that directly perturb the subject's trunk are limited with respect to the type of control (either kinematics or force) and the perturbation profiles that can be applied to perturb the subject. Most of these systems use variable drop weights as a means for delivering different perturbations and, hence, are able to generate solely *one particular force profile* in time [21,23-27,29,30]. Moreover, our team discovered after careful examination of the drop weight perturbation system that it does not generate impulse-like force profiles as desired [36].

After more than ten years of research in the field, our team became convinced that a portable device, which is able to generate diverse perturbations with variable intensities and profiles, is essential for a better understanding of postural control in able-bodied and disabled individuals. Therefore, our team has developed a portable and automated postural perturbation system (PAPPS) that can deliver arbitrary displacement, velocity, and force perturbations as a function of time. Note that this device could be used as a diagnostic tool, a research device, and a training system for enhancing balance in different patient populations. Due to the high modularity and flexibility of the PAPPS, it is applicable for a large range of postural scenarios such as sitting, standing, or treadmill walking. In addition, one can use a single or up to eight perturbation systems to deliver synchronized or consecutive perturbations in multiple directions. The objective of the present study was to report on the design of the PAPPS and to evaluate its performance in (1) accuracy and repeatability tests and (2) an exemplary postural perturbation application during sitting.

## II. MATERIALS AND METHODS

### A. *Design of the Postural Perturbation System*

The PAPPS was designed to elicit arbitrary displacement, velocity, or force perturbations at any desired height. The next key requirement was that the system is portable and that it can be easily transported (e.g., in a car) or mailed as a parcel. As a final requirement it had to be ensured that multiple systems can be connected in a daisy chain configuration to provide synchronized or consecutive perturbations in various directions. In particular, it was envisioned that up to eight PAPPS's may be connected in such a linked configuration. To meet these design requirements, the PAPPS had to be developed so that it consisted of 1) a conventional actuation system, 2) a custom-designed actuator control circuit and software that could control up to eight perturbation systems simultaneously, and 3) a custom-designed, light mechanical frame that not only holds and stabilizes the actuation system, but that can also be easily disassembled.

The horizontal perturbations provided by the PAPPS were delivered to the subject/patient via short stainless steel cables (one per PAPPS, i.e., perturbation direction), karabiners, and a soft, custom-made chest harness. The chest harness, which was 14 cm wide and 1.35 m long, was made of canvas and used heavy duty fasteners and Velcro strips for fixation. In addition, it had loops every 3 cm apart to accommodate the attachment of the stainless steel cables for different perturbation directions and chest sizes.

#### *1) Actuation System of the PAPPS*

The hardware configuration of the actuation system is schematically depicted in Fig. 1. The actuator was purchased as an assembled *Linear Servo Motor System* from Rotalec Inc. (Canada). It consisted of the TBX2508-D forcer, the TR25-875 magnetic tube

(Copley Controls Corp., Massachusetts, USA), SHW series internally lubricated linear bearings (THK, Japan), an MS-20 series optical encoder (RSF Electronics Inc., California, USA), and a custom-machined base plate and rod supports. The forcer was magnetically coupled to and driven along the rod. This particular forcer-rod combination could generate a peak displacement of 661 mm, a peak velocity of 0.5 m/s, and a peak force of 624 N. In addition, an iLoad Pro series *Load Cell* (Loadstart Sensors, California, USA) was attached to the system to facilitate force feedback control. It had a capacity of 250 lbs (113.4 kg) and an accuracy of 0.25 % of the full-range output (0.5-4.5 V). The optical encoder on the other hand had a resolution of 1  $\mu\text{m}$  and an accuracy of  $\pm 30 \mu\text{m}$ .

Power was provided to the system through a custom *Power Distribution Unit* (PDU) that was purchased from Interact Power (California, USA). The PDU was connected to a 43-Series *Control Panel* (Interact Power) that indicated the status of the main circuit breaker and included emergency OFF control. The PDU accepted 30 A per phase at 120 VAC (50-60 Hz) and provided 208 VAC and 24 A per phase output. It also served as a ground reference for the PAPPS frame and as a power source for the load cell.

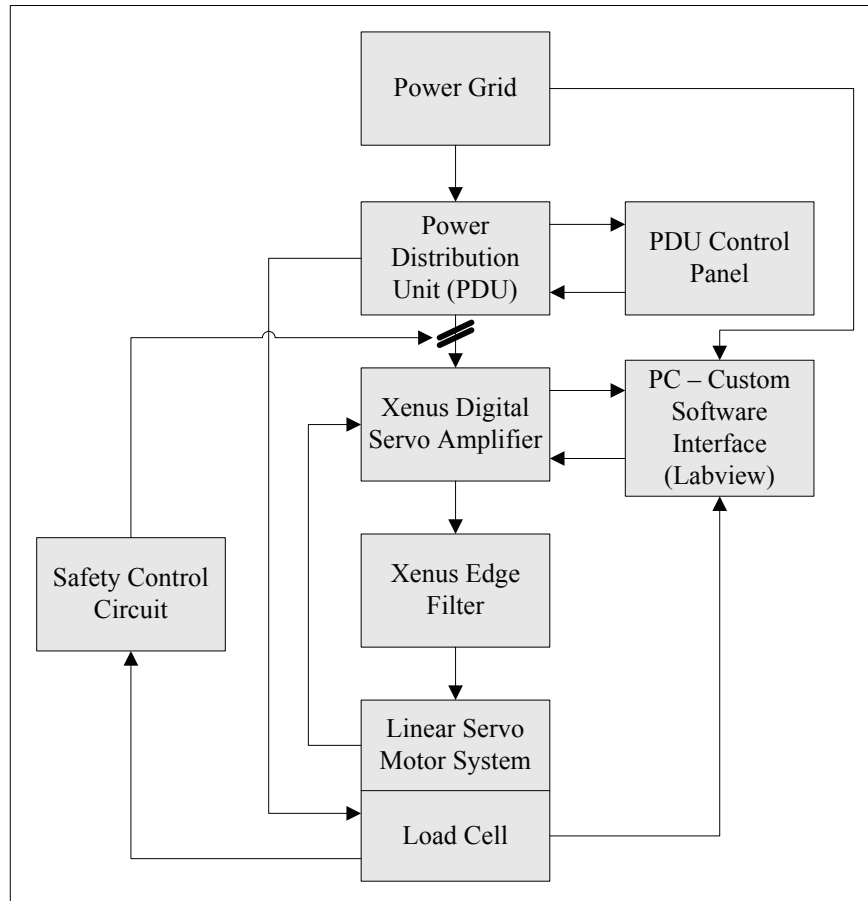


**Fig. 1.** Diagram of the PAPPS hardware configuration. The actuator was controlled using a custom software interface developed in LabVIEW, a Xenus digital servo amplifier, and a Xenus edge filter.

## 2) Control Circuit and Software of the PAPPS

As shown in the diagram of Fig. 1, the actuator was controlled using a *Custom Software Interface* developed in LabVIEW (version 8.0, National Instruments, Texas, USA), a *Xenus Digital Servo Amplifier* and a *Xenus Edge Filter* (Copley Controls Corp.). The servo amplifier had internal position, velocity, and current feedback control loops that operated at sampling frequencies of 3 kHz (position and velocity) and 15 kHz (current). The amplifier could operate in stand-alone mode according to a pre-programmed algorithm or be continuously updated from an external source using RS-232 communication. Since

the time delays associated with the data acquisition and LabVIEW processing permitted a maximum operating frequency of 100 Hz, the internal amplifier loops were used to control the actuator between PC updates. The edge filter was necessary to reduce the noise on the output side of the amplifier by increasing the rise time of the raw pulse-width modulated amplifier signal.

To ensure the safety of the subjects/patients who are perturbed by the PAPPS, an independent *Safety Control Circuit* was implemented. The circuit was monitoring the output of the load cell and severed the PDU power flow if the reading exceeded a predefined threshold level that depends on the application. The PAPPS was then disengaged and shut down instantaneously to prevent any form of injury. It is important to point out that this safety circuit was not the only safety layer of the PAPPS. Many other safety features were included in the system such as peak displacement, velocity, and force limits as well as maximum rates of change of the controlled variable. The circuit discussed in this section was the last-resort measure that would protect the subject/patient in an unlikely event that the PAPPS controller fails and causes unpredicted movement of the body.

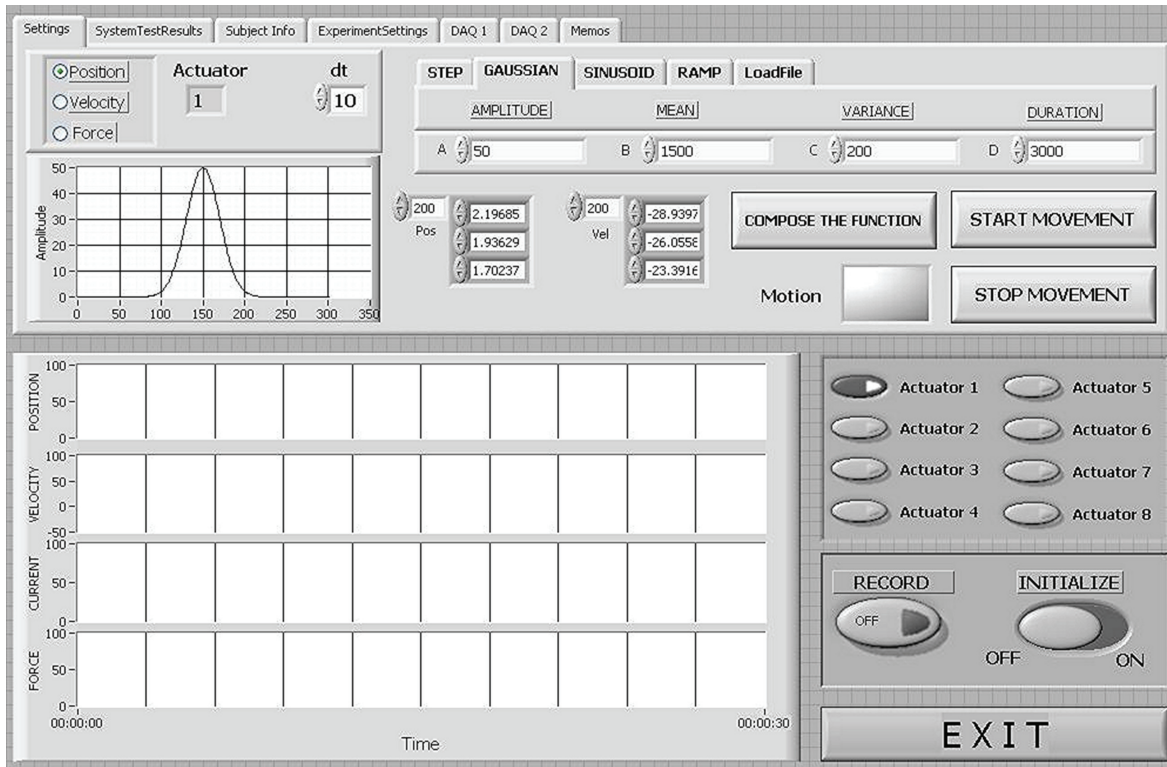


**Fig. 2.** Graphical user interface for controlling the PAPPs. After having selected the desired perturbation unit (actuators 1 to 8), the user could choose from different perturbation types and profiles. In addition, any arbitrary profile using a single column text file could be uploaded. During the perturbations, the measured position and velocity, the current commands to the servo amplifier, and the measured force were recorded for all active actuators and could be monitored (one actuator at a time).

Figure 2 shows the graphical user interface (GUI) implemented to control the PAPPs. The GUI, which was written using LabVIEW, allowed the user to select the type of perturbation, i.e., a position-, velocity-, or force-controlled perturbation. In addition, the user could choose from various forms of pre-programmed perturbation profiles. At the time of this study, the profile library consisted of sinusoidal, Gaussian (impulse), step, and ramp profiles, which can be easily expanded to include more complex perturbation profiles (e.g., pseudorandom profiles). In addition, the user can upload any arbitrary profile using a single column text file at a specified sampling frequency. Once the desired perturbation profile with particular parameters was selected and the actuator initialized, the system was

ready to deliver the perturbation to the subject/patient. During the perturbation, the measured actuator position and velocity, the current commands to the servo amplifier, and the measured force were recorded and could be monitored in real-time via the GUI.

In a daisy chain configuration of the PAPPS, the desired perturbation type and profile can be composed or uploaded for each perturbation unit separately (actuators 1 to 8 in Fig. 2). After this has been completed for all actuators, the synchronized perturbations could be executed via the universal '*Start Movement*' button (Fig. 2). Using CAN-bus and network addresses that are uniquely assigned to particular perturbation units, the control software will then send distinct commands to the units' actuators, allowing for virtually simultaneous motion control (inter-actuator delay in  $\mu\text{s}$ -range) and for actuator-coded data acquisition. Note that the described operation method in daisy chain configuration ensures, for example, that wire cables of passive actuators do not restrict the motion of the perturbed subject/patient by having the passive actuators simultaneously moved towards the subject/patient at the time of perturbation. Using a similar technique, two actuators opposite to each other can also execute sinusoidal perturbations as commonly delivered via movable surfaces.

### 3) *Mechanical Structure of the PAPPS*

A schematic and a photograph of the mechanical structure of the PAPPS are shown in Fig. 3. The light-weight mechanical frame, whose dimensions were 65.00"(H)  $\times$  36.75"(L)  $\times$  29"(W) (165.10 cm  $\times$  93.35 cm  $\times$  73.66 cm), was designed to allow the user to easily assemble and disassemble the device between usage and storage or shipping. The frame consisted of seven independent pieces that were tied together at eight points using M6 bolts. The pieces were: front (1) and rear (2) pillars, left (3) and right (4) base side

angles, the frame top (5), and left (6) and right (7) struts for enhanced stability. The linear actuator was mounted onto an actuator support plate (8), which was then coupled to the frame through support plate anchors (9) that slid vertically onto the pillars. The actuator support plate was attached to the support plate anchors with four M6 bolts and could be removed from the frame with the actuator attached to avoid disconnecting the wires from the actuator when the frame was to be dismantled. Note that the height of the support plate and, hence, of the actuator could be continuously adjusted by fixing the support plate anchors (9) at a desired height via two M6 bolts per side that pushed against the pillars. As a result, the height of the applied perturbation could range from as low as 20 cm to up to 160 cm. Note that Fig. 3 also shows a potential daisy chain configuration of the PAPPS that uses eight perturbation units.

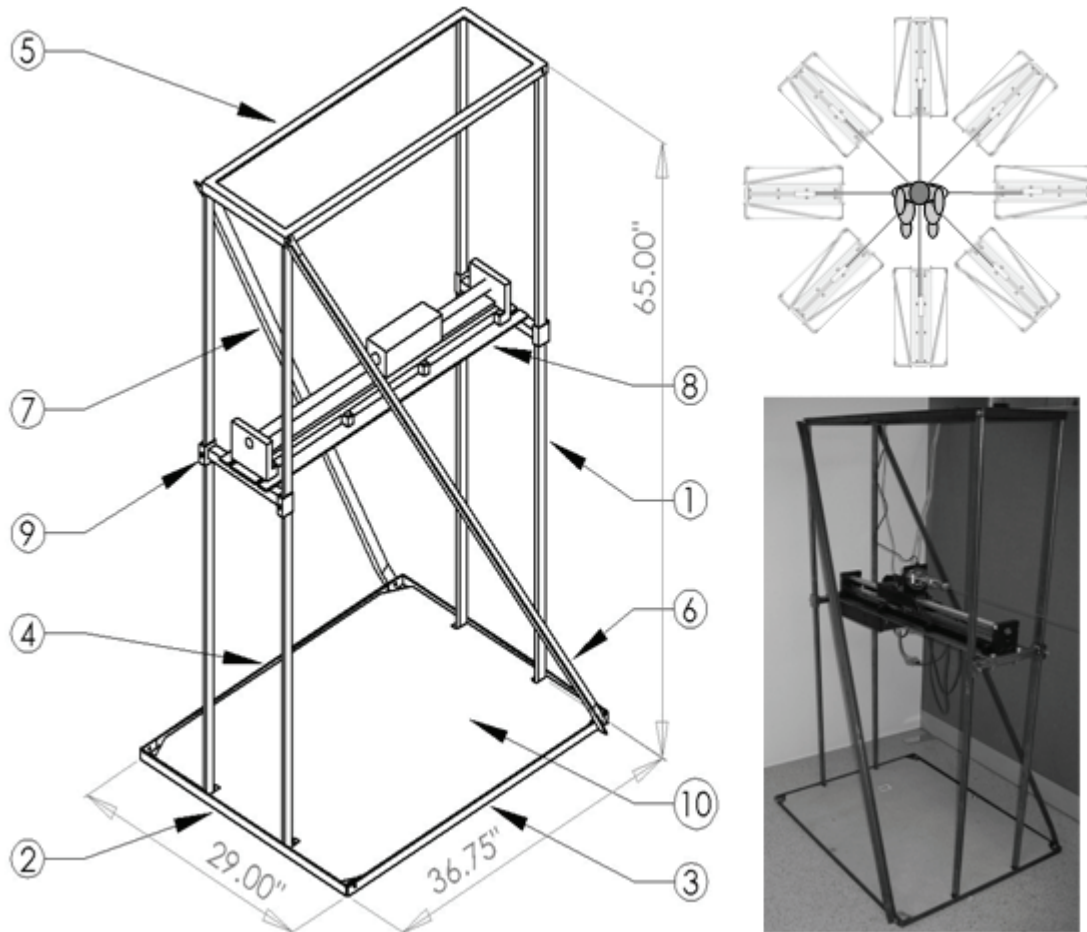


**Fig. 3.** Schematic, photograph and potential daisy chain configuration of the PAPPS (actuator and frame). The frame had a height of 65" (165.10 cm), a length of 36.75" (93.35 cm), and a width of 29" (73.66 cm). It was kept stationary during actual perturbations using friction: a wooden platform (10) was fixed onto the frame base and a large mass (~60 kg) was placed on top of it.

The frame was made from 1" × 1/2" × 0.065" (2.54 cm × 1.27 cm × 0.17 cm) rectangular steel tubes and 1" × 1" × 1/8" (2.54 cm × 2.54 cm × 0.32 cm) hot-rolled steel angles. The support plate was machined out of a 3/16" (0.48 cm) thick hot rolled steel sheet, whereas the support plate anchors were welded from a 1" × 1" × 0.065" (2.54 cm × 2.54 cm × 0.17 cm) square steel tube and two pieces of 1.5" × 3/4" (3.81 cm × 1.91 cm) rectangular steel tube. The frame was kept stationary during actual perturbations using friction: a wooden platform (10) was fixed onto the frame base and a large mass of

approximately 60 kg was placed on top of it. Note that this mass was found to be sufficient for frame stabilization independent of the weight of the subject and the type and profile of the perturbation.

### ***B. Accuracy and Repeatability Tests***

In order to evaluate the performance of the PAPPS, accuracy and repeatability tests were performed for position, velocity, and force control using the following perturbation profiles:

- Sinusoid
- Gaussian/Impulse
- Ramp/Step

As listed in Table 1, a variety of parameters (e.g., amplitude, frequency, and variance) was tested for each perturbation profile so as to cover the range of potential postural perturbation applications. During the tests, the actuator was positioned at a height of 90 cm, which marks the center of the applicable vertical range. In addition, the time difference between the perturbation command and the perturbation onset was recorded to capture the time delay of the system.

**Table 1.** Perturbation profiles, perturbation types, and applied parameters.

Perturbation		Sets	Amplitude	Frequency
Profile	Type			
Sinusoid	Position	6	0.5 / 2 / 4 [cm]	0.5 / 1 [Hz]
	Velocity	4	10 / 20 [cm/s]	0.5 / 1 [Hz]
	Force	2	12.5 / 25 [N]	0.25 [Hz]
Perturbation		Sets	Amplitude	Variance
Profile	Type			
Gaussian/ Impulse	Position	6	5 / 10 / 15 [cm]	0.15 / 0.3 [s]
	Velocity	4	10 / 20 / 40 [cm/s]	0.15 / 0.3 [s]
	Force	2	50 / 100 [N]	1 [s]
Perturbation		Sets	Amplitude	Rise Time
Profile	Type			
Ramp/ Step	Position	6	2.5 / 5 / 7.5 / 10 [cm]	0.25 / 0.5 / 1 [s]
	Velocity	3	5 / 10 [cm/s]	0.5 / 1 [s]
	Force	2	50 / 100 [N]	2 [s]

*1) Position-, Velocity-, and Force-Controlled Perturbations*

During the *position and velocity perturbation tests*, a drop weight of 20 lbs (9.1 kg) was attached to the actuator via the load cell, a stainless steel cable, and a pulley. Note that the drop weight, which could move freely, was used to simulate the resistive force that the actuator would encounter during position- or velocity-controlled postural perturbations. A highly sensitive laser displacement sensor with a measurement resolution of 10  $\mu\text{m}$  (LK2500, Keyence, Japan) was placed in line with the actuator to record the motion of the actuator during all trials. Note that the external measurements from the displacement sensor were used to: (1) verify the accuracy of the internal displacement and velocity measurements provided by the encoder of the PAPPS, and (2) identify whether an elastic deformation or translational motion of the PAPPS occurred during the perturbations. For each perturbation type and profile, three consecutive trials with the same profile

parameters were executed in order to evaluate the accuracy and repeatability of the perturbations.

During the *force perturbation tests*, the actuator was attached to the frame of the PAPPS via the load cell and a short stainless steel cable (*isometric force*). The force readings were sent back to the system for feedback and externally recorded for further analysis. As for the other tests, three consecutive trials were executed for each set of force profile parameters to evaluate the accuracy and repeatability of the perturbations. Note that the force profiles were executed in addition to a constant load (25 N or 50 N) to ensure a positive (pulling) force at all times.

## 2) Data Processing and Analysis

The measurements from the laser displacement sensor and the load cell were digitized at 1 kHz and converted into displacement and force, respectively. To eliminate high-frequency noise while preserving the key features of the measured profiles, the signals were then low-pass filtered using a fourth-order, zero phase-lag Butterworth filter with a cut-off frequency of 20 Hz. Finally, the actuator's velocity was calculated using

$$v[n]=0.5\cdot(x[n+1]-x[n-1])\cdot f_s, \quad (1)$$

where  $v[n]$  is the actuator's velocity at sample  $n$ ,  $x[n+1]$  the actuator's position at sample  $n+1$ , and  $f_s$  the sampling frequency (1 kHz). The internal position and velocity measurements of the PAPPS were digitized at 100 Hz and low-pass filtered the same way as the external measurements.

To quantify the performance *accuracy* of the PAPPS for all trials and all types of perturbation, the coefficient of determination ( $R^2$ ), the proportion of the variability of the

desired performance (given displacement, velocity, or force profile) that was accounted for by the actual performance (measured displacement, velocity, or force profile), was calculated. To quantify the performance *repeatability* of the PAPPS, the standard deviation of  $R^2$  was determined. Note that both the performance accuracy and performance repeatability were identified for each perturbation profile separately and for the sum of all trials.

### ***C. Example Application: Postural Perturbations during Sitting***

#### *1) Experimental Procedure*

Following the accuracy and repeatability tests, the PAPPS was used to demonstrate its capabilities in a case study with a single able-bodied individual. The healthy male subject was 24 years of age, had a height and weight of 190 cm and 90 kg, respectively, and reported no history of neurological disorders or chronic back pain. He gave written informed consent to the experimental procedure, which was approved by the ethics committees of the University of Toronto (Health Sciences) and the Toronto Rehabilitation Institute in accordance with the declaration of Helsinki on the use of human subjects in experiments. During the experiments, the participant was sitting on a stool in an upright position and was perturbed in the anterior direction at the level of his sternum. Note that the horizontal perturbations were delivered via the load cell, a short stainless steel cable, and the previously described chest harness (*see Section II A*). The perturbations were position-controlled and featured a profile that consisted of multiple full-wave sinusoids with pseudorandom frequency. The peak-to-peak amplitude was set to 10 mm, the frequencies ranged from 0.1 to 2.5 Hz, and the perturbation lasted for 30 s. Ten perturbation trials were performed during which the participant was instructed to maintain

an upright sitting posture as close as possible. Breaks of five minutes were given in between trials.

## *2) Data Acquisition and Processing*

During each trial, the motion of the actuator and the load on the system were recorded with the laser displacement sensor and the load cell, respectively. A second laser displacement sensor (LK2500, Keyence, Japan), which was positioned behind the subject at the height of his sternum, measured the anterior-posterior trunk motion. In addition, the electromyogram (EMG) of the right erector spinae at the level of the third lumbar vertebra (ES-L3) was recorded with a Bortec Biomedical AMT-8 EMG system and BiPole surface EMG electrodes (Bortec Biomedical Ltd., Canada). The EMG of ES-L3 was amplified by a factor of 1,000 and band-pass filtered between 10 and 1,000 Hz.

Due to the high frequency response range of the EMG system, all time series were digitized at a sampling frequency of 2 kHz. The EMG time series of ES-L3 were then rectified and filtered using a fourth-order, zero phase-lag Butterworth filter with a cut-off frequency of 2 Hz. The time series of the displacement sensors and the load cell were processed as described in Section B2. By applying Eq. (1) and  $f_s$  of 2 kHz, the data on the subject's trunk motion were finally used to compute the angular acceleration of the trunk around the hip joints (anterior-posterior degree of freedom) under the assumption that the trunk is rigid.

### III. RESULTS

#### A. *Position-Controlled Perturbations*

The results for the position-controlled sinusoidal perturbations with amplitudes and frequencies listed in Table 1 can be seen in Fig. 4. In each subplot, the bold gray lines represent the desired position of the actuator, whereas the thin black lines represent the actual position of the actuator. For each set of perturbation parameters, the individual time series from all three consecutive trials (not the average measurements) are depicted. Figures 4A and 4C show the internal measurements from the encoder and Figs. 4B and 4D the external measurements from the laser displacement sensor. The bold black vertical line at the beginning of each subplot indicates the average instant in time when the PAPPS was triggered to deliver the perturbation (*see also Figs. 5 to 8*). Note that the time difference between the trigger instant and the onset of the perturbation represents the overall system delay.

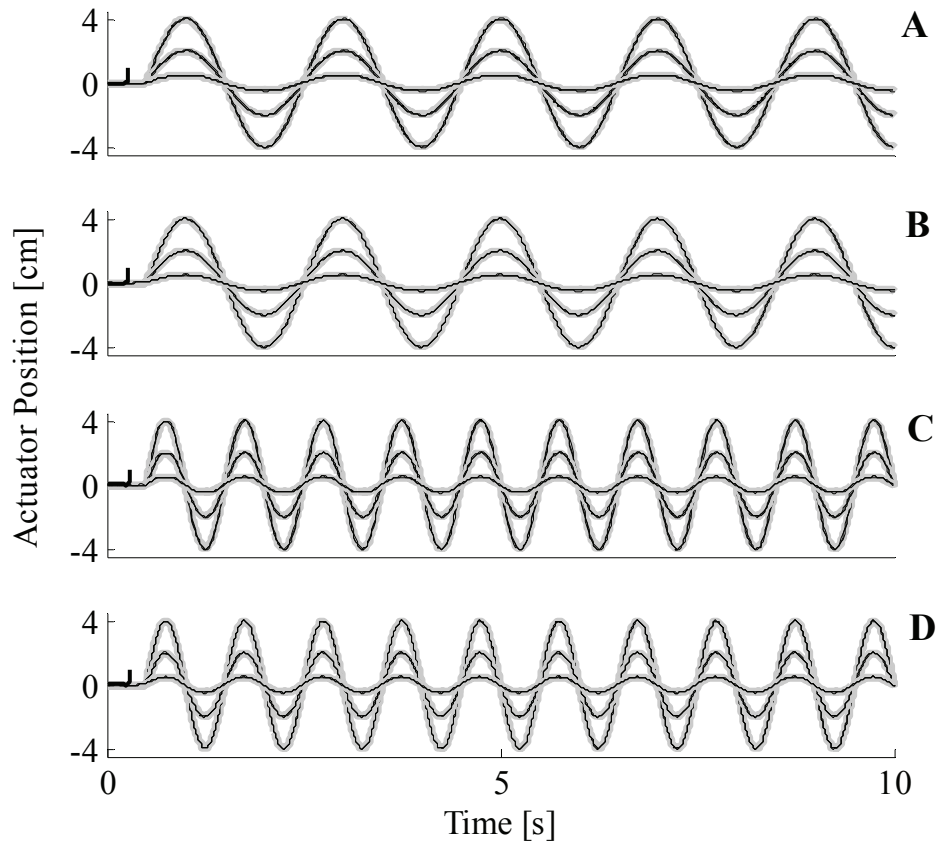


**Fig. 4.** Sinusoidal displacement perturbations with amplitudes and frequencies listed in Table 1. The bold gray lines mark the desired and the thin black lines the actual position of the actuator. Figures 4A and 4C show internal and Figs. 4B and 4D show external measurements.

Figure 5 shows the results for the position-controlled Gaussian and ramp profiles with amplitudes, variances (Gaussian), and rise times (ramp) described in Table 1. The subplots on the left side (Fig. 5A) show the internal measurements from the encoder and the subplots on the right side (Fig. 5B) the external measurements from the laser displacement sensor (thin black lines) in comparison to the desired position (bold gray lines). As in Fig. 4, all individual time series (not the average measurements) are depicted for each set of perturbation parameters.

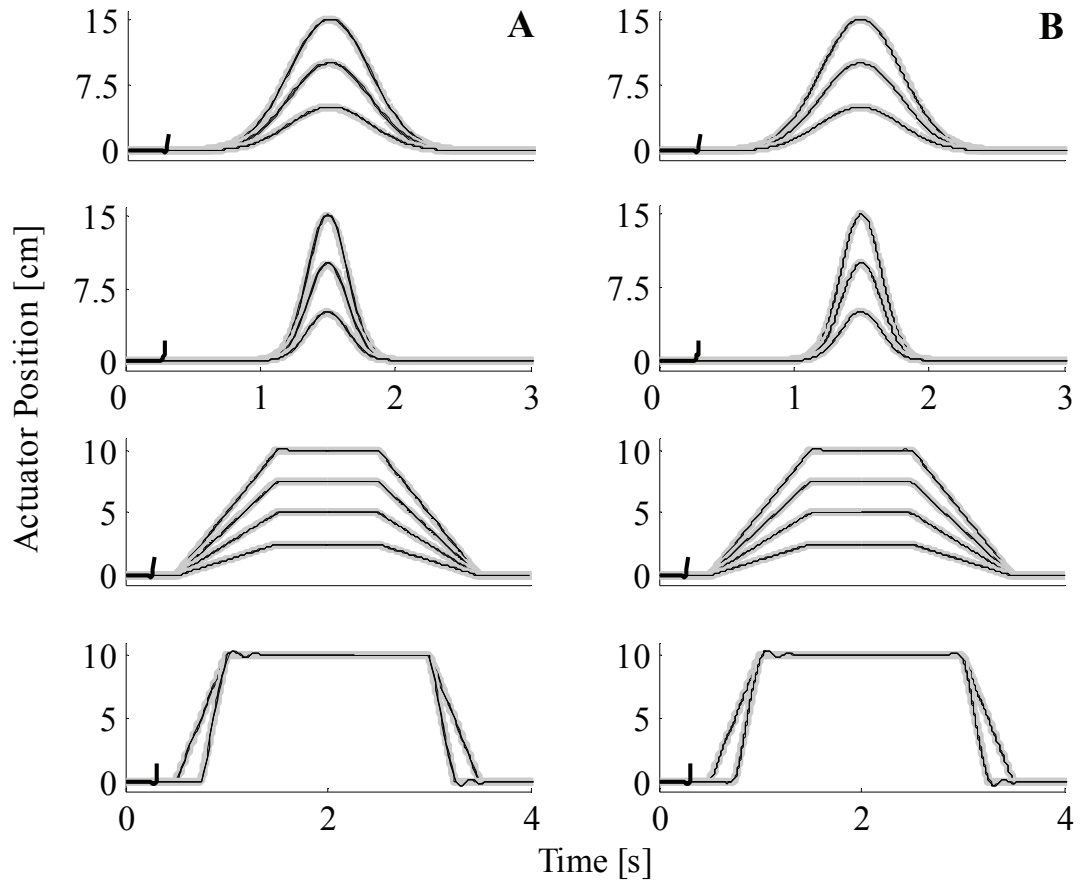


**Fig. 5.** Gaussian and ramp displacement perturbations with amplitudes, variances, and rise times described in Table 1. The bold gray lines mark the desired and the thin black lines the actual position of the actuator. The left subplots (Fig. 5A) show internal and the right subplots (Fig. 5B) show external measurements.

### ***B. Velocity-Controlled Perturbations***

The results for the velocity-controlled sinusoidal perturbations with amplitudes and frequencies listed in Table 1 can be seen in Fig. 6. Figures 6A and 6C show the internal measurements from the encoder and Figs. 6B and 6D the external measurements from the laser displacement sensor (thin black lines) in comparison to the desired velocity (bold gray lines). For each set of perturbation parameters, the individual time series from all three consecutive trials (not the average measurements) are depicted.

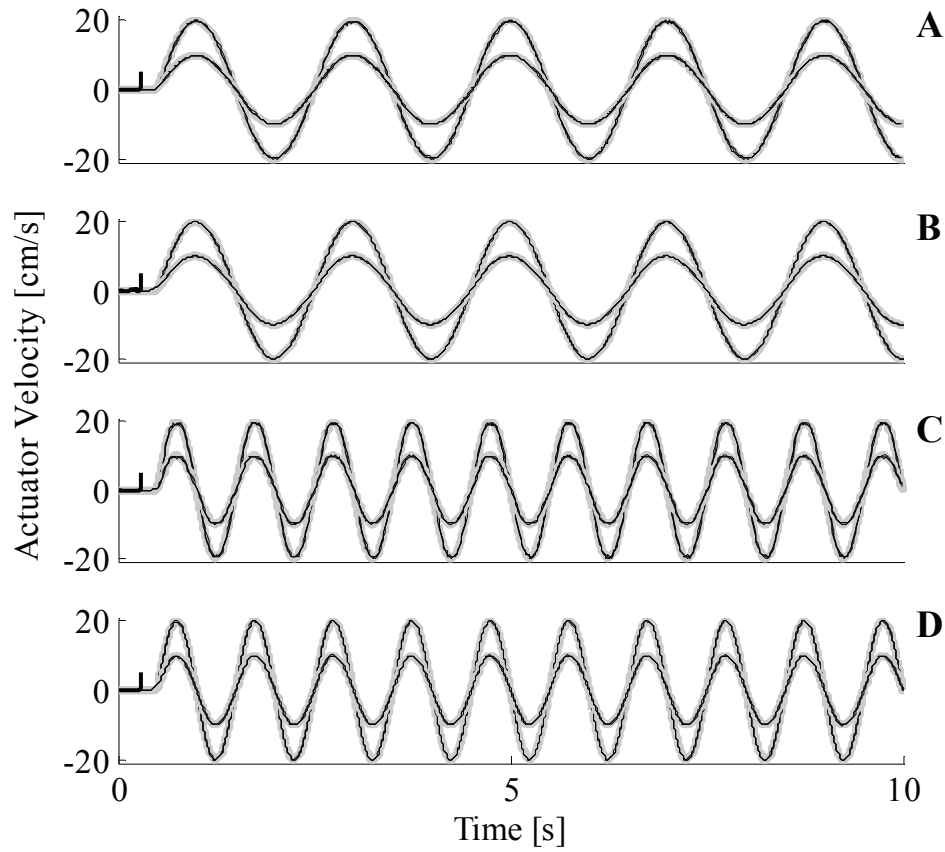


**Fig. 6.** Sinusoidal velocity perturbations with amplitudes and frequencies listed in Table 1. The bold gray lines mark the desired and the thin black lines the actual velocity of the actuator. Figures 6A and 6C show internal and Figs. 6B and 6D show external measurements.

Figure 7 shows the results for the velocity-controlled Gaussian and ramp perturbations with amplitudes, variances (Gaussian), and rise times (ramp) described in Table 1. The subplots on the left side (Fig. 7A) show the internal measurements from the encoder and the subplots on the right side (Fig. 7B) show the external measurements from the laser displacement sensor (thin black lines) in comparison to the desired velocity (bold gray lines). As in the previous figures, all individual time series (not the average measurements) are depicted for each set of perturbation parameters.

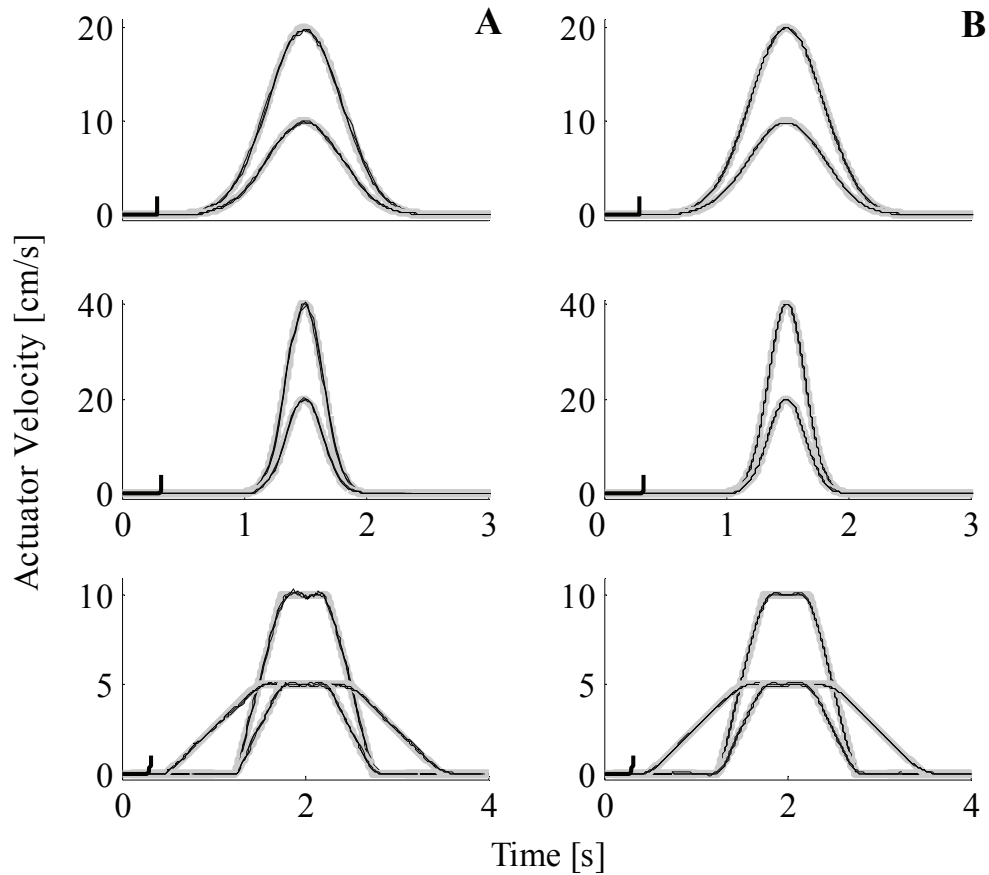


**Fig. 7.** Gaussian and ramp velocity perturbations with amplitudes, variances, and rise times described in Table 1. The bold gray lines mark the desired and the thin black lines the actual velocity of the actuator. The left subplots (Fig. 7A) show internal and the right subplots (Fig. 7B) show external measurements.

### C. Force-Controlled Perturbations

The results for the force-controlled perturbations with parameters listed in Table 1 can be seen in Fig. 8. In each subplot, the bold gray lines represent the desired isometric force, whereas the thin black lines represent the force measured by the load cell. Figures 8A, 8B, and 8C show the sinusoidal, the Gaussian, and the ramp perturbations, respectively. For each set of perturbation parameters, the individual time series from all three consecutive trials (not the average measurements) are depicted.

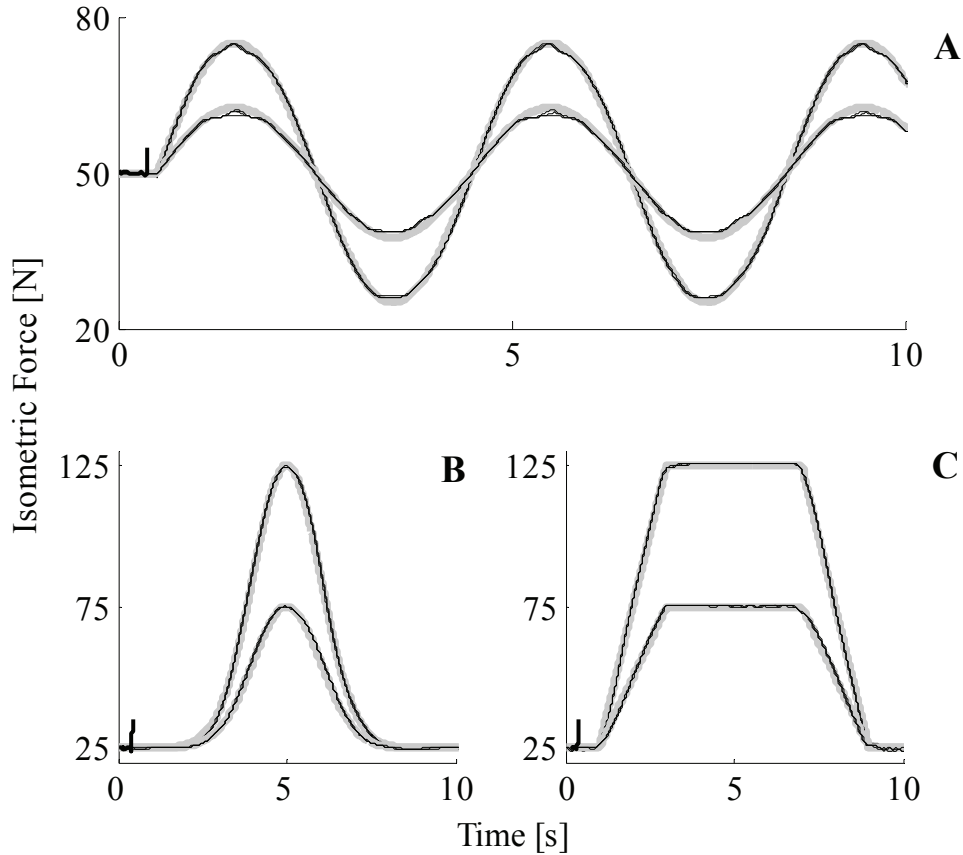


**Fig. 8.** Force perturbations with amplitudes, frequencies, variances, and rise times listed in Table 1. The bold gray lines mark the desired and the thin black lines the measured force on the system. Figures 8A, 8B, and 8C show the sinusoidal, the Gaussian, and the ramp perturbations, respectively.

#### ***D. Accuracy and Repeatability Results***

The results of the perturbation tests depicted in Figs. 4 to 8 reveal that the actual perturbation profiles fitted the desired perturbation profiles extremely well. As shown in Table 2, the coefficient of determination  $R^2$  proved to be very high for all perturbation types (displacement, velocity, and force) and perturbation profiles (mean of 99.9 %). This implies a high level of accuracy in the delivery of the PAPPS perturbations. Note that, in the case of the displacement and velocity perturbations, the internal measurements provided by the encoder and the external measurements provided by the laser displacement sensor matched exceptionally well. A two-sample t-test actually revealed that there was no

significant difference between the two measurement forms ( $p = 0.138$ ,  $t$ -statistic =  $-1.488$ , degrees of freedom = 190, equal variance assumption). In addition, the offsets between the internal and external measurements had a similar magnitude as the measurement resolution of the laser displacement sensor (*see Table 2 and Section IIB*). These findings suggest that (1) the PAPPS did not move during the perturbations regardless of the delivered perturbation, and (2) the accuracy of the sensors integrated within the PAPPS matches that of high quality sensors such as the one used in this study. Moreover, the low standard deviation in  $R^2$  of approximately 0.1 % indicates a high level of repeatability with respect to the perturbation delivery. In fact, during the sum of 105 trials, the PAPPS did not fail once to deliver high accuracy perturbations. Finally, it should be noted that the average time delay between the perturbation command and the perturbation onset was found to be  $201 \pm 16$  ms.

**Table 2.** Accuracy and repeatability results for the PAPPS.

Perturbation Type	Profile	Trials × Sets	R <sup>2</sup> Accuracy [%]		Offset [Int.-Ext.]
			Internal	External	
Position	Sinusoid	3 × 6	99.75 ± 0.20	99.93 ± 0.06	+4 μm
	Gaussian	3 × 6	99.98 ± 0.01	99.99 ± 0.00	-15 μm
	Ramp/Step	3 × 6	99.99 ± 0.01	99.99 ± 0.01	-13 μm
Velocity	Sinusoid	3 × 4	99.85 ± 0.10	99.96 ± 0.02	+7 μm/s
	Gaussian	3 × 4	99.96 ± 0.02	99.97 ± 0.02	-14 μm/s
	Ramp/Step	3 × 3	99.90 ± 0.01	99.90 ± 0.04	+14 μm/s
Force	Sinusoid	3 × 2	<i>NA</i>	99.63 ± 0.27	<i>NA</i>
	Gaussian	3 × 2	<i>NA</i>	99.83 ± 0.08	<i>NA</i>
	Ramp/Step	3 × 2	<i>NA</i>	99.85 ± 0.06	<i>NA</i>
Overall Mean ± S.D.:			99.90 ± 0.13	99.93 ± 0.11	

### ***E. Results of Postural Perturbation Case Study***

The time series recorded 5 s prior and 25 s after the onset of the pseudorandom sinusoidal displacement perturbations are depicted in Fig. 9 (case study). In the top subplot, the bold gray line represents the desired position of the actuator, whereas the thin black lines represent the measured actuator position during the ten executed trials (10 separate time series plotted on top of each other). In the second subplot, the load on the system as measured by the load cell is presented as an ensemble average for all ten trials. The third subplot shows the ensemble-averaged angular acceleration of the subject's trunk around the hip joints (anterior-posterior degree of freedom), with a positive acceleration indicating trunk acceleration in the forward direction. The last two subplots depict the ES-L3 activity, first as an ensemble-averaged envelope (fourth subplot) and then as a raw EMG signal (bottom subplot).

The plots in Fig. 9 reveal a distinct relationship between the perturbations, the load on the system, the trunk acceleration, and the recorded muscle activity. In addition, it can be seen that the trunk acceleration and the ES-L3 activity (third and fourth subplots) preceded the perturbation and load fluctuation (first and second subplots) as captured with the dotted lines. This observation was verified by cross-correlation analysis, which indicated that the average ES-L3 activity preceded the average actuator displacement by 159 ms ( $r = 0.79$ ).

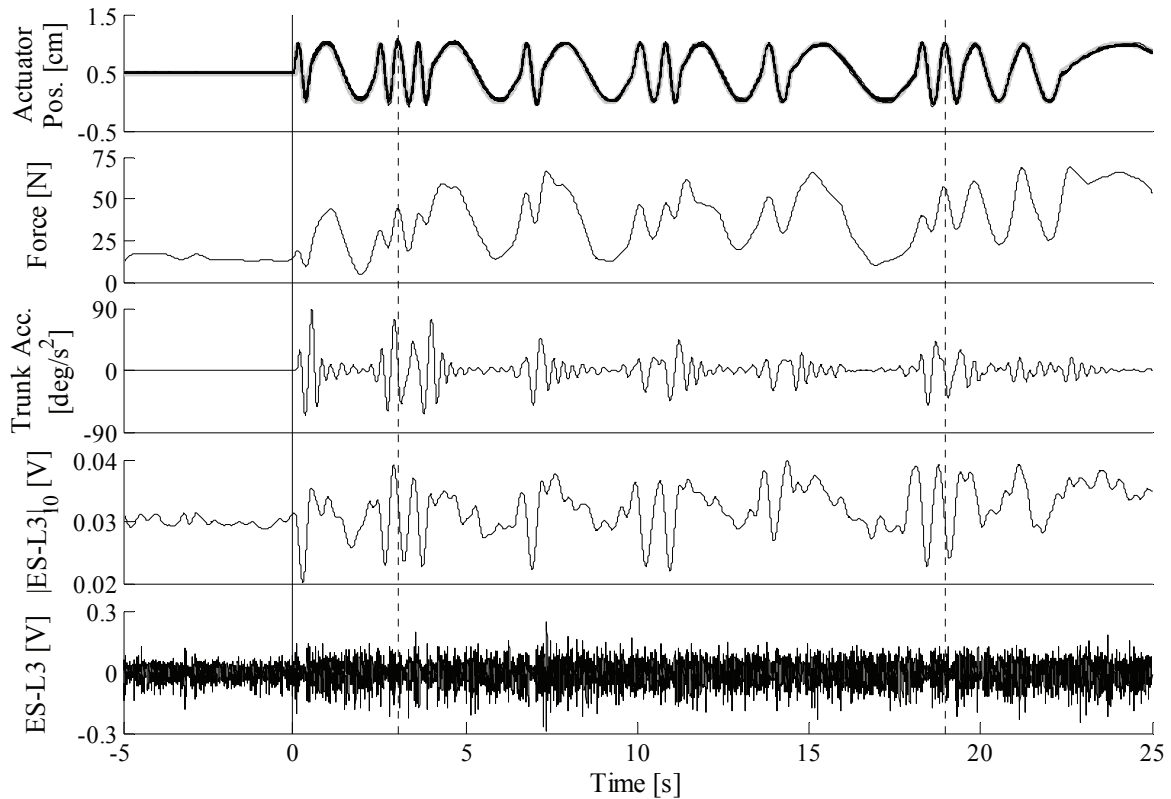


**Fig. 9.** Actuator displacement (top row), average load cell force (second row), average trunk acceleration (third row), average ES-L3 activity (fourth row), and raw ES-L3 activity (bottom row) during pseudorandom sinusoidal displacement perturbations. The dotted lines mark instants in time at which the advance of trunk acceleration and ES-L3 activity with respect to actuator position and force can be easily seen.

## IV. DISCUSSION

### A. *Technical Performance of the PAPPS*

The results of the accuracy and repeatability tests clearly demonstrate that the PAPPS is a reliable, high-precision device for delivering postural perturbations. Although the PAPPS was designed for maximum portability and modularity, it can cover a vertical range of horizontal perturbations from as low as 20 cm to up to 160 cm. As a result, it can be used for a wide range of subject/patient anthropometrics and postural scenarios found in the scientific literature. Moreover, it exhibits displacement, velocity, and force perturbation capabilities that exceed the needs of postural perturbation experiments or training. It is also important to stress that potential users can use a single or multiple perturbation systems in order to create complex perturbation scenarios. The PAPPS was actually designed to allow eight perturbation units to act in a daisy chain configuration (*see Fig. 3*), which is a unique feature not available in competing perturbation systems. Note that a similar device has been used to evoke protective sidestepping in young and older adults [32]; however, it seems more limited with respect to 1) the number of perturbation lines (six versus eight), 2) the available perturbation types (kinematics versus kinematics and force), and 3) the potential for complex experimental protocols including synchronized perturbations.

The PAPPS control system is user-friendly as the user can select the desired perturbation type, perturbation profile, and respective parameters in a few steps via a straightforward GUI. In addition, the PAPPS permits synchronization with other experimental systems such as EMG, motion analysis, and force plate systems. It is also important to note that the external measurements verified the accuracy of the PAPPS and that no elastic deformations and/or translational motion occurred during the perturbations. The high accuracy of the internal measurements from the encoder finally implies that no

external measurement devices are needed to capture the kinematics of the PAPPS during action.

### ***B. Scientific Potential of the PAPPS***

Since the body of literature related to postural perturbations indicates that the postural response elicited by a perturbation is dependent on the mechanical interaction between the perturbing force and the current mechanical state of the body, one purpose of the PAPPS is to afford maximum independent control over the mechanical perturbation. By diligently controlling this component of the interaction, it will be possible to enhance the understanding of the actual mechanical properties of the body during and following perturbation. Analysis of the acquired data (e.g., EMG and kinematics), along with computer modeling approaches, will then allow researchers to study how both the passive structural and active neuromuscular properties of the system contribute to the observed postural response.

Several studies have emphasized that it is important to control the properties of the perturbation. Diener *et al.* [37] as well as Runge *et al.* [38] showed that the kinematic parameters of the perturbation have a significant influence on the body's linked-segment kinetics and neuromuscular (EMG) response. Others have found that a typical ramp displacement profile used in surface perturbations actually produces two separate perturbations (initial acceleration and subsequent deceleration), each of which affects the elicited postural response [39]. Finally, it has been shown that the postural response after perturbation is greatly affected by the direction of perturbation [12,14,15].

By carefully controlling the properties of the perturbation, a wide range of physiological questions can be addressed using the PAPPS. It still remains open, for

example, what kind of postural perturbation responses are primarily pre-programmed and which responses are mostly integrated based on sensory feedback information. In addition, it is unclear to what extent postural responses are determined by the biomechanical properties and constraints of the body [40]. Note that other research questions will come to the foreground as more is understood of how the human body utilizes available balance control strategies dependent on factors such as the state of the body and the characteristics of the perturbation.

### ***C. Case Study and its Scientific Potential***

The main purpose of the performed case study was to demonstrate an example of how the PAPPS could be applied in postural perturbation studies. Such a study could not only be used to investigate postural responses to mechanical perturbations, but also for more sophisticated scientific paradigms, including the identification of particular reflex dynamics (e.g., [20-22]) and of stiffness properties of various body segments (e.g., [18,19]). In this context, a more sophisticated device for perturbation delivery is particularly valuable for its potential to enhance the outcome of studies that use experimental data to identify, support, or reject a theoretical relationship of dependence. To give an example, the data from the presented case study could be used to characterize the relationship between load and muscle activity, to identify the time delays in the physiological feedback control system, and to investigate the nature of the underlying postural control mechanism during sitting or standing.

## V. CONCLUSIONS

The portable and automated postural perturbation system (PAPPS) was developed to help scientists and clinicians gain a better insight into postural control in more realistic environments. Instead of bringing subjects/patients to the gait laboratories, one can easily take the PAPPS to the community and perform postural assessments in novel settings. A need for such a system has been identified some time ago by our research team at the Toronto Rehabilitation Institute, and the PAPPS is the first attempt to address this need. The PAPPS is a portable and very accurate perturbation system that can deliver arbitrary displacement, velocity, and force perturbations. The perturbations were delivered horizontally and with a vertical range from as low as 20 cm to up to 160 cm. As a result, the PAPPS could be used to test postural responses during sitting, standing, treadmill walking, etc. Besides the postural response studies, the PAPPS could be used to assess and train balance in patients with neuromuscular disorders or to perform neuromuscular system identification experiments. Since up to eight perturbation devices can be connected and simultaneously controlled in a daisy chain configuration, the PAPPS is well suited for complex perturbation experiments requiring sophisticated perturbation profiles and temporal fidelity when these perturbations are delivered.

## **ACKNOWLEDGMENT**

The authors thank Dr. Richard Preuss for his helpful comments on the revised version of the manuscript. This work was supported by the Canadian Institutes of Health Research (#HSF-86427), the Natural Sciences and Engineering Research Council of Canada (#249669), the Toronto Rehabilitation Institute, and the University of Toronto.

## REFERENCES

- [1] Horak, F. B., 1987, "Clinical measurement of postural control in adults," *Phys. Ther.*, 67, pp. 1881–1885.
- [2] Horak, F. B., Henry, S. M., and Shumway-Cook, A., 1997, "Postural perturbations: new insights for treatment of balance disorders," *Phys. Ther.*, 77, pp. 517–533.
- [3] Maki, B. E., Holliday, P. J., and Fernie, G. R., 1990, "Aging and postural control. A comparison of spontaneous- and induced-sway balance tests," *J. Amer. Ger. Soc.*, 38, pp. 1–9.
- [4] Maki, B. E., and Ostrovski, G., 1993, "Do postural responses to transient and continuous perturbations show similar vision and amplitude dependence?," *J. Biomech.*, 26, pp. 1181–1190.
- [5] Horak, F. B., Shupert, C. L., Dietz, V., and Horstmann, G., 1994, "Vestibular and somatosensory contributions to responses to head and body displacements in stance," *Exp. Brain Res.*, 100, pp. 93–106.
- [6] McIlroy, W. E., and Maki, B. E., 1996, "Age-related changes in compensatory stepping in response to unpredictable perturbations," *J. Geront.*, 51, pp. M289–296.
- [7] Peterka, R. J., 2002, "Sensorimotor integration in human postural control," *J. Neurophysiol.*, 88, pp. 1097–1118.
- [8] Forssberg, H., and Hirschfeld, H., 1994, "Postural adjustments in sitting humans following external perturbations: muscle activity and kinematics," *Exp. Brain Res.*, 97, pp. 515–527.

- [9] Hirschfeld, H., and Forssberg, H., 1994, "Epigenetic development of postural responses for sitting during infancy," *Exp. Brain Res.*, 97, pp. 528–540.
- [10] Zedka, M., Kumar, S., and Narayan, Y., 1998, "Electromyographic response of the trunk muscles to postural perturbation in sitting subjects," *J. Electromyogr. Kinesiol.*, 8, pp. 3–10.
- [11] Hedberg, Å., Forssberg, H., and Hadders-Algra, M., 2004, "Postural adjustments due to external perturbations during sitting in 1-month-old infants: evidence for the innate origin of direction specificity," *Exp. Brain Res.*, 157, pp. 10–17.
- [12] Carpenter, M. G., Allum, J. H. J., and Honegger, F., 1999, "Directional sensitivity of stretch reflexes and balance corrections for normal subjects in the roll and pitch planes," *Exp. Brain Res.*, 129, pp. 93–113.
- [13] Bloem, B. R., Allum, J. H. J., Carpenter, M. G., Verschuur, J. J. G. M., and Honegger, F., 2002, "Triggering of balance corrections and compensatory strategies in a patient with total leg proprioceptive loss," *Exp. Brain Res.*, 142, pp. 91–107.
- [14] Henry, S. M., Fung, J., and Horak, F. B., 1998, "Control of stance during lateral and anterior/posterior surface translations," *IEEE Trans. Neural Sys. Rehab. Eng.*, 6, pp. 32–42.
- [15] Henry, S. M., Fung, J., and Horak, F. B., 1998, "EMG responses to maintain stance during multidirectional surface translations," *J. Neurophysiol.*, 80, pp. 1939–1950.
- [16] Torres-Oviedo, G., and Ting, L. H., 2007, "Muscle synergies characterizing human postural responses," *J. Neurophysiol.*, 98, 2144–2156.

- [17] Carpenter, M. G., Tokuno, C. D., Thorstensson, A., and Cresswell, A. G., 2008, “Differential control of abdominal muscles during multi-directional support-surface translations in man,” *Exp. Brain Res.*, 188, 445–455.
- [18] Gardner-Morse, M. G., and Stokes, I. A. F., 2001, “Trunk stiffness increases with steady-state effort,” *J. Biomech.*, 34, pp. 457–463.
- [19] Lee, P. J., Rogers, E. L., and Granata, K. P., 2006, “Active trunk stiffness increases with co-contraction,” *J. Electromyogr. Kinesiol.*, 16, pp. 51–57.
- [20] Fitzpatrick, R., Burke, D., and Gandevia, S. C., 1996, “Loop gain of reflexes controlling human standing measured with the use of postural and vestibular disturbances,” *J. Neurophysiol.*, 76, pp. 3994–4008.
- [21] Granata, K. P., Slota, G. P., and Bennett, B. C., 2004, “Paraspinal muscle reflex dynamics,” *J. Biomech.*, 37, pp. 241–247.
- [22] Moorhouse, K. M., and Granata, K. P., 2007, “Role of reflex dynamics in spinal stability: intrinsic muscle stiffness alone is insufficient for stability,” *J. Biomech.*, 40, pp. 1058–1065.
- [23] Krajcarski, S. R., Potvin, J. R., and Chiang, J., 1999, “The in vivo dynamic response of the spine to perturbations causing rapid flexion: effects of pre-load and step input magnitude,” *Clin. Biomech.*, 14, pp. 54–62.
- [24] Cholewicki, J., Simons, A. P. D., and Radebold, A., 2000, “Effects of external trunk loads on lumbar spine stability,” *J. Biomech.*, 33, pp. 1377–1385.

- [25] Radebold, A., Cholewicki, J., Polzhofer, G. K., and Greene, H. S., 2001, "Impaired postural control of the lumbar spine is associated with delayed muscle response times in patients with chronic idiopathic low back pain," *Spine*, 26, pp. 724–730.
- [26] Granata, K. P., Slota, G. P., and Wilson, S. E., 2004, "Influence of fatigue in neuromuscular control of spinal stability," *Human Factors*, 46, pp. 81–91.
- [27] Thomas, J. S., Lavender, S. A., Corcos, D. M., and Andersson, G. B. J., 1998, "Trunk kinematics and trunk muscle activity during a rapidly applied load," *J. Electromyogr. Kinesiol.*, 8, pp. 215–225.
- [28] Stokes, I. A. F., Gardner-Morse, M., Henry, S. M., and Badger, G. J., 2000, "Decrease in trunk muscular response to perturbation with preactivation of lumbar spinal musculature," *Spine*, 25, pp. 1957–1964.
- [29] Radebold, A., Cholewicki, J., Panjabi, M. M., and Patel, T. C., 2000, "Muscle response pattern to sudden trunk loading in healthy individuals and in patients with chronic low back pain," *Spine*, 25, pp. 947–954.
- [30] Vera-Garcia, F. J., Brown, S. H. M., Gray, J. R., and McGill, S. M., 2006, "Effects of different levels of torso coactivation on trunk muscular and kinematic responses to posteriorly applied sudden loads," *Clin. Biomech.*, 21, pp. 443–455.
- [31] Pai, Y.-C., Rogers, M. W., Patton, J., Cain, T. D., and Hanke, T. A., 1998, "Static versus dynamic predictions of protective stepping following waist-pull perturbations in young and older adults," *J. Biomech.*, 31, pp. 1111–1118.

- [32] Patton, J. L., Hilliard, M. J., Martinez, K., Mille, M.-L., and Rogers, M. W., 2006, "A simple model of stability limits applied to sidestepping in young, elderly and elderly fallers," *Conf. Proc. IEEE Eng. Med. Biol. Soc.*, 1, pp. 3305–3308.
- [33] Do, M. C., Breniere, Y., and Brenguier, P., 1982, "A biomechanical study of balance recovery during the fall forward," *J. Biomech.*, 15, pp. 933–939.
- [34] Do, M. C., Breniere, Y., and Bouisset, S., 1988, "Compensatory reactions in forward fall: are they initiated by stretch receptors?," *Electroencephalogr. Clin. Neurophysiol.*, 69, pp. 448–452.
- [35] <http://www.neurocomplatform.com/> (February 22, 2008).
- [36] Sin, V. W. H., 2007, "Muscle recruitment patterns during sitting," M.A.Sc. thesis, University of Toronto, Canada.
- [37] Diener, H. C., Horak, F. B., and Nashner, L. M., 1988, "Influence of stimulus parameters on human postural responses," *J. Neurophysiol.*, 59, pp. 1888–1905.
- [38] Runge, C. F., Shupert, C. L., Horak, F. B., and Zajac, F. E., 1999, "Ankle and hip postural strategies defined by joint torques," *Gait and Posture*, 10, 161–170.
- [39] Carpenter, M. G., Thorstensson, A., and Cresswell, A. G., 2005, "Deceleration affects anticipatory and reactive components of triggered postural responses," *Exp. Brain Res.*, 167, pp. 433–445.
- [40] Kuo, A. D., and Zajac, F. E., 1993, "Human standing posture: multi-joint movement strategies based on biomechanical constraints," *Prog. Brain Res.*, 97, pp. 349–358.

## Table Legends

**Table 1.** Perturbation profiles, perturbation types, and applied parameters.

**Table 2.** Accuracy and repeatability results for the PAPPS.

## Figure Legends

**Fig. 1.** Diagram of the PAPPS hardware configuration. The actuator was controlled using a custom software interface developed in LabVIEW, a Xenus digital servo amplifier, and a Xenus edge filter.

**Fig. 2.** Graphical user interface for controlling the PAPPS. After having selected the desired perturbation unit (actuators 1 to 8), the user could choose from different perturbation types and profiles. In addition, any arbitrary profile using a single column text file could be uploaded. During the perturbations, the measured position and velocity, the current commands to the servo amplifier, and the measured force were recorded for all active actuators and could be monitored (one actuator at a time).

**Fig. 3.** Schematic, photograph and potential daisy chain configuration of the PAPPS (actuator and frame). The frame had a height of 65” (165.10 cm), a length of 36.75” (93.35 cm), and a width of 29” (73.66 cm). It was kept stationary during actual perturbations using friction: a wooden platform (10) was fixed onto the frame base and a large mass (~60 kg) was placed on top of it.

**Fig. 4.** Sinusoidal displacement perturbations with amplitudes and frequencies listed in Table 1. The bold gray lines mark the desired and the thin black lines the actual position of the actuator. Figures 4A and 4C show internal and Figs. 4B and 4D show external measurements.

**Fig. 5.** Gaussian and ramp displacement perturbations with amplitudes, variances, and rise times described in Table 1. The bold gray lines mark the desired and the thin black lines the actual position of the actuator. The left subplots (Fig. 5A) show internal and the right subplots (Fig. 5B) show external measurements.

**Fig. 6.** Sinusoidal velocity perturbations with amplitudes and frequencies listed in Table 1. The bold gray lines mark the desired and the thin black lines the actual velocity of the actuator. Figures 6A and 6C show internal and Figs. 6B and 6D show external measurements.

**Fig. 7.** Gaussian and ramp velocity perturbations with amplitudes, variances, and rise times described in Table 1. The bold gray lines mark the desired and the thin black lines the actual velocity of the actuator. The left subplots (Fig. 7A) show internal and the right subplots (Fig. 7B) show external measurements.

**Fig. 8.** Force perturbations with amplitudes, frequencies, variances, and rise times listed in Table 1. The bold gray lines mark the desired and the thin black lines the measured force on the system. Figures 8A, 8B, and 8C show the sinusoidal, the Gaussian, and the ramp perturbations, respectively.

**Fig. 9.** Actuator displacement (top row), average load cell force (second row), average trunk acceleration (third row), average ES-L3 activity (fourth row), and raw ES-L3 activity (bottom row) during pseudorandom sinusoidal displacement perturbations. The dotted lines mark instants in time at which the advance of trunk acceleration and ES-L3 activity with respect to actuator position and force can be easily seen.